Quinone Electrophiles Selectively Adduct "Electrophile Binding Motifs" within Cytochrome *c*†

Ashley A. Fisher,[‡,§] Matthew T. Labenski,[‡,§] Srinivas Malladi,[||,⊥] Vijay Gokhale,[‡] Martina E. Bowen,[‡,§] Rania S. Milleron,[||] Shawn B. Bratton,[||,⊥] Terrence J. Monks,[‡,§] and Serrine S. Lau*[,‡,§]

Department of Pharmacology and Toxicology, College of Pharmacy, The University of Arizona, Tucson, Arizona 85721, Southwest Environmental Health Sciences Center, The University of Arizona, Tucson, Arizona 85721, and Division of Pharmacology and Toxicology, College of Pharmacy, and Institute for Cellular and Molecular Biology, The University of Texas, Austin, Texas 78712

Received March 30, 2007; Revised Manuscript Received June 22, 2007

ABSTRACT: Electrophiles generated endogenously, or via the metabolic bioactivation of drugs and other environmental chemicals, are capable of binding to a variety of nucleophilic sites within proteins. Factors that determine site selective susceptibility to electrophile-mediated post-translational modifications, and the consequences of such alterations, remain largely unknown. To identify and characterize chemical-mediated protein adducts, electrophiles with known toxicity were utilized. Hydroquinone, and its mercapturic acid pathway metabolites, cause renal proximal tubular cell necrosis and nephrocarcinogenicity in rats. The adverse effects of HQ and its thioether metabolites are in part a consequence of their oxidation to the corresponding electrophilic 1,4-benzoquinones (BQ). We now report that BQ and 2-(*N*-acetylcystein-*S*-yl)benzoquinone (NAC-BQ) preferentially bind to solvent-exposed lysine-rich regions within cytochrome *c*. Furthermore, we have identified specific glutamic acid residues within cytochrome *c* as novel sites of NAC-BQ adduction. The microenvironment at the site of adduction governs both the initial specificity and the structure of the final adduct. The solvent accessibility and local pK_a of the adducted and neighboring amino acids contribute to the selectivity of adduction. Postadduction chemistry subsequently alters the nature of the final adduct. Using molecular modeling, the impact of BQ and NAC-BQ adduction on cytochrome *c* was visualized, revealing the spatial rearrangement of critical residues necessary for protein−protein interactions. Consequently, BQ-adducted cytochrome *c* fails to initiate caspase-3 activation in native lysates and also inhibits Apaf-1 oligomerization into an apoptosome complex in a purely reconstituted system. In summary, a combination of mass spectroscopic, molecular modeling, and biochemical approaches confirms that electrophile−protein adducts produce structural alterations that influence biological function.

Cells are exposed to reactive electrophiles generated from a variety of sources, including byproducts of oxidative metabolism. Peroxidation of lipid membranes results in the formation of electrophilic aldehydes, and reactive carbonyl species such as glyoxal and 3-methylglyoxal are products of glycolysis. The ability of electrophilic carbonyl species to form protein adducts has been implicated in a number of disease processes, including diabetes, atherosclerosis, and neurodegenerative diseases. In a similar fashion, naturally occurring electrophiles present in the environment, and those formed via the metabolism of xenobiotics, can form covalent adducts with proteins. The technical challenges involved in the identification of such xenobiotic-derived protein adducts have limited the ability to determine their biological and/or toxicological significance. Nonetheless, such chemical-induced post-translational modifications (PTMs)[1] can alter the structure of proteins, with consequences that may alter protein function. These functional alterations may include interference with protein−protein interactions and subcellular protein localization, and disruption of cellular signaling pathways (*1*, *2*). Characterization of chemical-induced PTMs has been accomplished previously by detection techniques

† This work was supported by a grant from the National Institutes of Health (GM070890), by an NIEHS grant to the Southwest Environmental Health Sciences Center (ES06694) (all to S.S.L.), and by American Cancer Society Grant RSG-05-029-01-CCG (S.B.B.). T32 Training Grants ES007091 and CA09480 supported M.E.B. and R.S.M., respectively.

* To whom correspondence should be addressed: Southwest Environmental Health Sciences Center, Department of Pharmacology and Toxicology, College of Pharmacy, The University of Arizona, P.O. Box 210207, 1703 E. Mabel St., Tucson, AZ 85721. Telephone: (520) 626-0460. Fax: (520) 626-6944. E-mail: lau@pharmacy.arizona.edu.

‡ Department of Pharmacology and Toxicology, College of Pharmacy, The University of Arizona.

§ Southwest Environmental Health Sciences Center, The University of Arizona.

|| Division of Pharmacology and Toxicology, College of Pharmacy, The University of Texas.

⊥ Institute for Cellular and Molecular Biology, The University of Texas.

[1] Abbreviations: AMC, 7-amino-4-methylcoumarin; Apaf-1, apoptotic protease activating factor 1; BQ, 1,4-benzoquinone; CD, circular dichroism; CID, collision-induced dissociation; DEVD-AMC, *N*-acetyl-aspartate-glutamate-valine-aspartate-AMC; EBM, electrophilic binding motif; ESI, electrospray ionization; γ-GT, γ-glutamyl transpeptidase; GSBQ, (glutathion-*S*-yl)-1,4-benzoquinone; GSH, glutathione; LC−MS/MS, liquid chromatography with electrospray tandem mass spectrometry; MALDI, matrix-assisted laser desorption ionization; NAC-BQ, 2-(*N*-acetylcystein-*S*-yl)benzoquinone(s); NAC-HQ, 2-(*N*-acetylcystein-*S*-yl)hydroquinone(s); P-Mod, protein modification; PTMs, post-translational modifications; ROS, reactive oxygen species; TGHQ, 2,3,5-tris(glutathion-*S*-yl)hydroquinone.

10.1021/bi700613w CCC: $37.00
Published on Web 09/07/2007

such as Western analysis and radiolabeling, and more recently by utilizing mass spectrometry analysis (*3*, *4*). This latter mode of analysis has typically occurred at the amino acid level of proteins, for characterization of the chemically reactive species and for location of the exact amino acids which are modified on the protein (*3*). Several chemical toxicants capable of covalently modifying proteins have electrophilic properties. As a result, nucleophilic sites—such as cysteine thiols, lysine amines, histidine imidazoles, and protein N-terminal amines—are potential targets for the reactive electrophilic toxicants (*2*, *5*).

Quinones represent an extensive class of electrophilic molecules that can form covalent adducts with proteins and can produce toxicological effects via such adduction. Quinones are also capable of redox cycling and, consequently, of producing reactive oxygen species (*6*) and a subsequent oxidative stress (*7*−*9*). Because of the nucleophilicity of cysteinyl sulfhydryls, protein and nonprotein sulfhydryls are key targets of electrophilic quinone molecules. Glutathione (GSH), the major cellular nonprotein sulfhydryl, generally serves as a cytoprotectant because reactive electrophiles can covalently bind to its nucleophilic sulfhydryl, thus sparing the covalent modification of cellular macromolecules (*3*, *8*). 1,4-Benzoquinone (BQ) is an example of a reactive quinone that is an environmental toxicant. BQ is formed through oxidation of benzene, a low-molecular weight hydrocarbon and an environmental pollutant. Because of the electrophilic nature of BQ, several GSH molecules can be conjugated to BQ through the GSH free sulfhydryl (*3*, *6*, *10*, *11*). The conjugation of BQ with one GSH results in 2-(glutathion-*S*-yl)BQ (GSBQ). Subsequent conjugation with GSH results in the formation of multisubstituted GSH conjugates of BQ (*12*). BQ and its quinol-thioether metabolites cause renal proximal tubular cell necrosis, and 2,3,5-tris(glutathion-*S*-yl)hydroquinone (TGHQ) is nephrocarcinogenic in the Eker rat; these effects are mediated by their ability to generate ROS and their protein-arylation capabilities (*13*−*15*).

Although full characterization of chemically induced PTMs represents a significant challenge, recent advances in mass spectrometry and bioinformatics have increased the likelihood of success in detecting such PTMs. We have used cytochrome *c* as a model protein for in vitro adduction with BQ and NAC-BQ (selected to minimize the metabolic complexity of utilizing TGHQ) to characterize the covalent protein binding of these compounds and to demonstrate the influence of such chemical-induced PTMs on protein structure and function. Modification of cytochrome *c* by BQ has been previously demonstrated in our laboratory, where this electrophilic toxicant binds to solvent-exposed lysine-rich regions of the protein (*4*). We will be using BQ adduction on cytochrome *c* to gain an understanding of the role this chemical adduction plays in potential protein structural and functional changes. Cytochrome *c* was selected as a model protein to map the interaction between proteins and the electrophilic toxicants because it is structurally well characterized by NMR and X-ray crystallography. Additionally, cytochrome *c* contains no free sulfhydryls, so the adduction of the electrophilic toxicants to non-sulfhydryl nucleophiles can be analyzed (*3*). Furthermore, because cytochrome *c* is an integral component in the apoptosis pathway, the selective adduction of certain residues on the protein may influence its biological function. One necessary pathway for the induction of apopotosis involves formation of the multiprotein apoptosome complex. During apoptosis, cytochrome *c* is released from mitochondria and binds to cytosolic apoptosis protease activating factor 1 (Apaf-1), with subsequent recruitment and activation of initiator caspase-9 and effector caspase-3 and -7, thus forming the apoptosome (*16*, *17*).

Following chemical adduction, cytochrome *c* was analyzed by MALDI-MS and LC−MS/MS, followed by database mining algorithms and manual validation to identify the site specificity and types of adduction. Molecular modeling was then utilized to predict the structural modifications imposed upon the protein following the BQ and NAC-BQ adductions. We demonstrate that the chemical adduction of cytochrome *c* is site-specific and that postadduction chemistry dictates final adduct formation. Knowledge of this postadduction chemistry is critical in identifying site-specific PTMs. Additionally, we demonstrate that these PTMs cause a change in structure that leads to changes in protein function.

MATERIALS AND METHODS

Chemicals. 1,4-Benzoquinone (BQ), trifluoroacetic acid (TFA), and silver oxide were purchased from Aldrich (Milwaukee, WI); NAC-HQ was synthesized and purified as described previously (*12*). HPLC-grade solvents were purchased from EMD Chemicals. Horse heart cytochrome *c*, sequencing-grade trypsin, and all other reagents were from Sigma (St. Louis, MO).

1,4-Benzoquinone Modification on Cytochrome c. Horse heart cytochrome *c* was dissolved in deionized distilled water at a concentration of 1 mg/mL. BQ was dissolved in methanol at a concentration of 5 mg/mL. Cytochrome *c* was reacted with BQ at a molar ratio of 1:10 at room temperature for 30 min. The mixture was centrifuged at 5000*g* for 1 h through a Millipore Microcon 10 000 Da molecular mass cutoff centrifugal filter to remove excess BQ. The control and treated cytochrome *c* samples were spotted onto the MALDI target, and whole protein spectra were acquired.

Oxidation of NAC-HQ to NAC-BQ. NAC-HQ was dissolved in deionized distilled water with 0.1% TFA at a concentration of 50 mg/mL. Approximately 5 mg of silver oxide was added, and the solution was vortexed for 1 min. The solution was filtered through a 0.2 μm syringe filter. The solution was then purified by HPLC. A Shimadzu HPLC system (LC-10AS) was used with a UV−vis spectrophotometric detector (280 nm) and an Ultrasphere ODS C_{18} column (5 μm packing, 10 mm × 25 cm, Beckman-Coulter). The mobile phase consisted of acetic acid, methanol, and water (1:10:89, v/v). Aliquots of oxidized NAC-BQ (25 μL) were injected into the HPLC system and separated isocratically at a rate of 3.0 mL/min. The product eluted at 12.4 min. The yellow product was then analyzed by ESI-MS on a Finnigan MAT TSQ 7000 triple-quadrupole mass spectrometer (ThermoElectron, San Jose, CA). NAC-BQ was the dominant product (*m*/*z* 269).

NAC-BQ Modification on Cytochrome c. Horse heart cytochrome *c* (1 mg) was dissolved into buffers (1 mL) at pH 6 (50 mM ammonium bicarbonate and 50 mM ammonium acetate), pH 7 (100 mM ammonium bicarbonate), and pH 8 (100 mM ammonium bicarbonate). Aliquots were taken from each cytochrome *c* solution prior to NAC-BQ addition for use as control samples. NAC-BQ was dissolved

in deionized distilled water at 5 mg/mL. Each cytochrome *c* solution was reacted with NAC-BQ at a 1:10 molar ratio at room temperature for 30 min. The mixture was filtered once through a Millipore Microcon 10 000 Da molecular mass cutoff centrifugal filter for 1 h at 5000*g* to remove excess NAC-BQ. The control and treated samples were spotted on the MALDI target, and whole protein spectra were acquired. The samples were then digested for 6 h with sequencing-grade trypsin at a 1:50 (w/w) ratio at 37 °C in the dark. The digested samples (control and treated) were analyzed by LC−MS/MS.

MALDI-TOF. Prior to MALDI-MS analysis, samples were desalted using a C_{18} 0.6 mL ZipTip (Millipore, Bedford, MA), with 0.1% formic acid in water as the equilibration buffer and 1% formic acid in 50% acetonitrile/water as the elution buffer, following the manufacturer's protocol. MALDI-TOF spectra were recorded on an Applied Biosystems Proteomic Solution 1 System instrument with a 2 m flight path in the positive ion mode. The instrument was equipped with a nitrogen laser operating at 337 nm. Standard method parameters were used with a delay time of 200 ns. The solutions were diluted 1:1 in α-cyano-4-hydroxycinnamic acid, and 1 μL was drop-dried on a target plate. Whole protein spectra were acquired in linear mode over the mass range of 1000−100000 Da, where the spectra were sequentially stacked, and internal calibration was done with the cytochrome *c* peak.

LC−MS/MS. Cytochrome *c* was digested as described above, and peptides were separated via microbore HPLC (Magic 2002, Michrom BioResources, Auburn, CA) on a freshly packed 0.5 mm × 50 mm MAGIC MS C_{18} column (5 μm, 200 Å pore size) using a mobile phase of methanol, water, acetic acid, and trifluoroacetic acid, A (2:98:0.1:0.02) and B (10:90:0.09:0.02), with a gradient from 5 to 65% B over 30 min at a flow rate of 5 nL/min. The HPLC system was coupled on-line with an electrospray ion trap mass spectrometer (Finnigan-MAT LCQ Classic, Finnigan, San Jose, CA), set to a positive mode spray voltage of 3.5 kV and capillary temperature of 200 °C. The maximum injection time was 50 ms for a full scan and 200 ms for five MS/MS microscans. Dependent data setting was performed with a default charge of 2, an isolation width of 2 amu, an activation amplitude of 35%, an activation time of 30 ms, and a minimal signal of 50 000 ion counts. Global dependent data settings were as follows: reject mass width of 1 amu, dynamic exclusion enabled, exclusion mass width of 3 amu, repeat count of 3, repeat duration of 1 min, and exclusion duration of 1 min. Scan event series included one full scan with a mass range of 400−2000 Da, followed by one dependent MS/MS scan of the most intense ion. Mass spectrometer scan functions and HPLC solvent gradients were controlled by the Xcalibur data system (ThermoFinnigan, San Jose, CA).

Identification and Confirmation of Modified Tryptic Peptides. The protein sequence of cytochrome *c*, CYC_HORSE P00004, was obtained from the NCBI database. Peptide sequences were identified using the open-source search engine X! Tandem, which correlates the MS/MS spectra with amino acid sequences in a user-specified NCBI database (*18*, *19*). P-Mod was used to confirm the X! Tandem data, including the identification of spectra displaying characteristics of BQ or NAC-BQ adductions. P-Mod is an algorithm that screens data files for MS/MS spectra corresponding to peptide sequences in a search list. Modification of the primary peptide sequence shifts the peptide mass, which may be experimentally observed as a difference between the measured mass of the modified peptide precursor ion (adjusted for charge state) and the predicted mass of the unmodified peptide. The mass shift also will be observed in the *m*/*z* values of fragment ions containing the modified amino acid. Scores with *P* values of >0.01 were discarded as false positives (*20*). Upon collision-induced dissociation (CID) of the peptides, b- and y-ion fragments are generated: the b-ion series represents cleavage of the peptide bond and corresponds to the N-terminus, and y-ions result from cleavage of the amide bonds and contain the C-terminus (*21*). Manual validation of MS/MS spectra was then used to confirm the peptide sequence and adduct mass location. Peptides identified as being adducted by both X! Tandem and P-Mod were then manually validated using IonGen (trademark to SSL, The University of Arizona). IonGen generates theoretical b- and y-ions for user-specified peptides containing an adduct. This program facilitates faster, more accurate validation of adducted peptides. Only adducted peptides identified from X! Tandem, P-Mod, and manual validation with IonGen were used.

Molecular Modeling. The X-ray crystal structure coordinates for the horse cytochrome *c* structure from Protein Data Bank entry 1HRC were used as a starting model to build BQ- and NAC-BQ-adducted cytochrome *c* (*22*). Molecular modeling studies were carried out using the Biopolymer module of Insight II modeling software (Accelrys, Inc.) (*23*). BQ-cyclized diquinone and NAC-BQ were both built from the fragment library, and each adduct was formed on the appropriate residues of the protein. The charges were assigned using extensible systematic force field (ESFF) parameters (*24*). The modified structures were then subjected to 1000 steps of minimization using Discover 3.0. The complex structure was then soaked within a 10 Å layer of TIP3P water molecules (*25*). This assembly was then subjected to equilibration for 40 ps and dynamic simulations for 100 ps. Trajectories were collected every 0.1 ps. The lowest-potential energy structure was selected and then minimized using 3000 steps of minimization. The final minimized structure was then used for analysis. The NAC-BQ-adducted cytochrome *c* structures were viewed and manipulated using PyMOL (DeLano Scientific, LLC). The lowest-potential energy conformation of the NAC-BQ-adducted cytochrome *c*, constructed using Insight II, was then placed in PyMOL. Spatial rearragement of critical residues within cytochrome *c* as a consequence of NAC-BQ adduction was assessed by overlaying the adducted models with a native model of cytochrome *c*.

Circular Dichroism Spectroscopy. Circular dichroism measurements of native cytochrome *c*, BQ-adducted cytochrome *c*, and NAC-BQ-adducted cytochrome *c* were taken at 20 μM on a Jasco-810 spectropolarimeter (Jasco, Easton, MD) in 100 μM Tris-HCl at pH 7.5 using a quartz cell with an optical path length of 1.0 mm over a wavelength range of 180−260 nm. Each CD signal is the average of three scans at room temperature. The CD spectra are baseline-corrected, and the signal contributions due to the buffer were subtracted.

Cell Culture and Preparation of Cell Lysates. The human monocytic THP.1 tumor cell line was maintained at 37 °C in RPMI 1640 medium supplemented with 10% heat-inactivated fetal calf serum, 100 units/mL penicillin, and 100

mg/mL streptomycin, in an atmosphere of 5% CO_2 and 95% air. THP.1 cells were resuspended in lysis buffer containing 50 mM PIPES/KOH (pH 6.5), 150 mM KCl, 2 mM EDTA, 0.1% (w/v) CHAPS, 5 mM dithiothreitol, 20 mg/mL leupeptin, 10 mg/mL pepstatin A, 10 mg/mL aprotinin, and 2 mM phenylmethanesulfonyl fluoride. The cells were frozen in liquid nitrogen and thawed three times to ensure complete lysis and then centrifuged (45 min at 4 °C) at 20000*g* and 100000*g* to obtain cytosolic lysates. The protein concentration of the lysates was determined by the Bradford assay (Bio-Rad Laboratories, Hercules, CA).

Inhibition of Apoptosome Function by BQ-Modified Cytochrome c. In vitro activation of the Apaf-1 apoptosome was initiated by incubating human monocytic THP.1 lysates (10 mg/mL, protein concentration) for 30 min at 37 °C with 2 mM dATP, 2 mM $MgCl_2$, and various concentrations of BQ-adducted cytochrome *c* or native cytochrome *c* (2−40 μM). The ability of adducted and unadducted cytochrome *c* to initiate formation of the Apaf-1 apoptosome and sequential activation of caspase-9 and -3 in human monocytic THP.1 tumor cell lysate was assessed by measuring caspase-3 DEVDase activity. Because the apoptosome recruits and activates caspase-9 and -3, the indirect activation of the complex was detected by measuring caspase-3 DEVDase activity (*16*). Caspase-3 activity was measured as the ability to cleave the fluorophore 7-amino-4-methylcoumarin (AMC) from the caspase-3 target sequence, *N*-acetyl-aspartate-glutamate-valine-aspartate-AMC (DEVD-AMC), as previously described (*26*). Liberation of AMC from DEVD was monitored continuously using 380 nm excitation and 460 nm emission. Lysates were assayed for DEVDase activity in caspase assay buffer [0.1% CHAPS, 10 mM dithiothreitol, 100 mM HEPES, and 10% sucrose (pH 7.0)]. The reaction was started with 20 μM DEVD-AMC, and the reaction was followed for 2−4 min. The DEVDase activity was calculated and expressed as picomoles per milligram of protein per minute. His-tagged caspase-9 was expressed in *Escherichia coli* BL21(DE3)-pLysS, and His-tagged Apaf-1XL and procaspase-3 were expressed using a baculovirus-mediated insect cell (Hi-Five) expression system. Caspase-9, caspase-3, and Apaf-1XL were purified with a Ni-NTA (Qiagen) affinity column, followed by MonoQ anion-exchange chromatography. Caspase-9 (200 nM) and Apaf-1XL (200 nM) were incubated with either cytochrome *c* or BQ-adducted cytochrome *c* (10 μM), along with dATP (10 μM) and DEVD-AMC for 5 min at room temperature in 20 μL of caspase assay buffer. The reaction was initiated by adding procaspase-3 (500 nM), and the rate of release of AMC was measured using a Victor^3 plate reader (Perkin-Elmer). For gel filtration assays, Apaf-1XL oligomerization was induced using either cytochrome *c* or BQ-adducted cytochrome *c* (10 μM) along with dATP (10 μM) for 20 min at room temperature in a final reaction volume of 200 μL. The reaction sample was then loaded onto a Superose 6 10/300 GL column (GE Healthcare), pre-equilibrated with buffer [20 mM Hepes, 50 mM NaCl, and 1 mM DTT (pH 7.5)] at 4 °C. Fractions (500 μL) were collected and further analyzed by immunoblotting with a rabbit polyclonal Apaf-1XL antibody.

RESULTS

Predicted Protein Conformational Changes Associated with 1,4-BQ Modification. BQ may induce conformational changes in cytochrome *c*, possibly altering residues involved in Apaf-1 binding, and thus inhibiting apoptosome formation. Previous site-directed mutagenesis studies showed that cytochrome *c* forms complexes with Apaf-1 via an annulus of lysine residues on K^7, K^{25}, K^{39}, ^{62}ETLM^{65}, and K^{72}. Because the LC−MS/MS analysis indicated that BQ forms a cyclized diquinone adduct on specific lysine residues (*4*), the BQ structure was built to mimic this binding to cytochrome *c*. The cyclized diquinone adduct is the formation of one BQ molecule on a lysine residue and the formation of another BQ molecule on an adjacent lysine residue. These two BQ molecules adjoin to form one adduct with a mass of 196 Da (*4*). With the cyclized BQ addition to K^{25}−K^{27} of cytochrome *c*, the protein conformation changed to accommodate this molecule, modifying the bond distance of lysine residues 25−27 from 5.26 Å in the native conformation to 9.27 Å with the addition of cyclized BQ (Figure 1). The residues in cytochrome *c* that interact with Apaf-1 are highlighted in this model, and following adduction of cyclic BQ to K^{25}−K^{27}, the specific residues involved in interaction with Apaf-1 exhibit spatial rearrangement.

Adduction of NAC-BQ to Cytochrome c at pH 6, 7, and 8. To determine the mechanism by which NAC-BQ mediates chemically induced PTMs, cytochrome *c* was adducted by NAC-BQ at a 1:10 molar ratio at pH 6, 7, and 8. Following the adduction, MALDI spectra were recorded for the control and treated whole proteins at each pH (*3*). The control spectra of cytochrome *c* showed a peak at *m*/*z* 12 360, which corresponds to the mass of the native protein. No additional peaks were present in each of the control samples (data not shown). The MALDI spectrum of cytochrome *c* adducted by NAC-BQ at pH 6 shows the native cytochrome *c* at *m*/*z* 12 360 and several additional peaks corresponding to the addition of NAC-BQ to the protein. NAC-BQ will modify the protein with a mass addition of 268 Da, and the peaks at *m*/*z* 12 628, 12 897, and 13 168 correspond to one, two, and three NAC-BQ additions, respectively, on cytochrome *c* at pH 6 (Figure 2A). At pH 7, the MALDI spectrum of cytochrome *c* adducted by NAC-BQ shows a similar pattern of multiple 268 Da additions of NAC-BQ on the protein as seen at pH 6. However, this sample also exhibits several additions of 105 Da, which is indicative of postadduction thioether loss and apparent BQ addition (106 Da) on cytochrome *c*. The peak at *m*/*z* 12 465 corresponds to a 105 Da mass addition, and the peak at *m*/*z* 12 732 corresponds to a mass addition of 105 + 268 Da (Figure 2B). The MALDI spectrum of cytochrome *c* modified by NAC-BQ at pH 8 identifies the most abundant modification as the mass addition of 105 Da (Figure 2C).

These samples were then subjected to tryptic digestion and LC−MS/MS analysis to characterize the NAC-BQ adduct formation on cytochrome *c*. Peptide sequences were identified using X! Tandem database searching followed by P-Mod analysis and manual validation. Following the reaction at pH 6 (as stated in Materials and Methods), six peptides were identified as having an addition of 268 Da (Table 1). The 268 Da addition was found on either lysine or glutamic acid residues within these peptides. The peptide ^{61}EETLMEYLENPKK^{73} was one of the tryptic peptides with the 268 Da addition; for this peptide, the addition was identified on K^{72}. The modification is isolated to the C-terminal portion of the

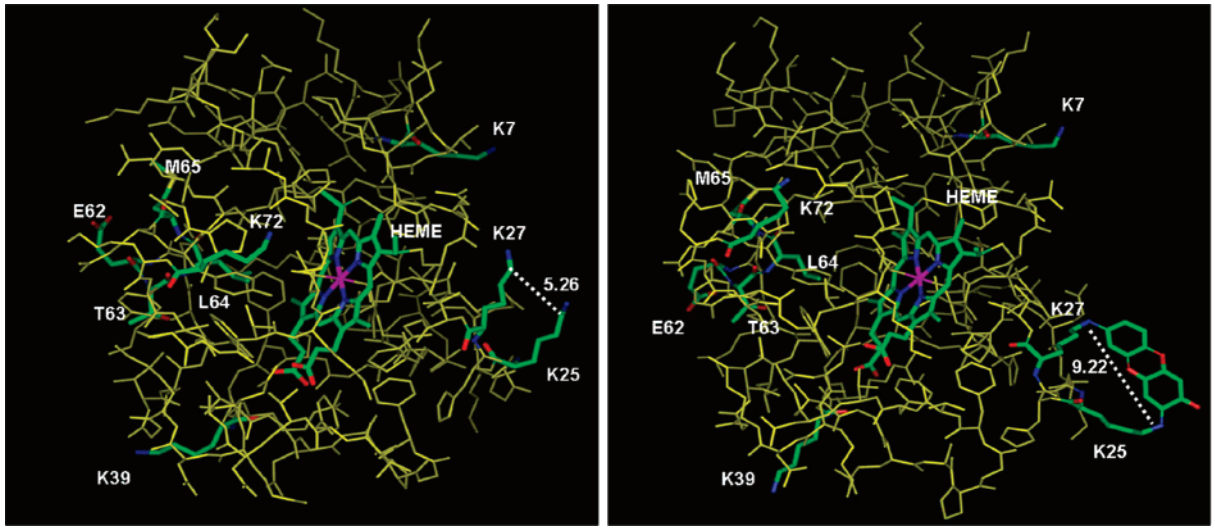

FIGURE 1: Structural modification of cytochrome *c* as a result of BQ adduction. MS/MS data showed a 194 Da BQ adduct on $K^{25}-K^{27}$ of cytochrome *c*. The model was derived from the coordinates of the protein structure of Protein Data Bank entry 1HRC, and Insight II was used to build the adducted protein. Following adduction with the BQ molecule, the distance between K^{25} and K^{27} has corrected for the addition. Native cytochrome *c* has a $K^{25}-K^{27}$ bond distance of 5.26 Å (left), and BQ-adducted cytochrome *c* has a $K^{25}-K^{27}$ bond distance of 9.22 Å (right). Several of the residues involved in the Apaf-1−cytochrome *c* interaction are impacted by the adduction to $K^{25}-K^{27}$ and are highlighted in green.

peptide (amino acids 71−73); however, the modification most likely resides on K^{72}, because adduction at K^{73} would prevent tryptic cleavage at this site, thus creating a larger peptide. Additionally, the peptide ^{39}KTGQAPGFTYTDANK^{53} had the 268 Da addition on K^{39}. The peptide ^{92}EDLIAYLKK^{100} had the 268 Da addition on E^{92} (Figure 3A). The glutamic acid residue is a novel site of adduction and is specific to the pH 6 reaction. The b-ion series of this peptide shows a mass shift at several b-ions that indicate E^{92} as the site of the 268 Da addition. The y-ion series of this peptide indicate no mass shift at the C-terminal portion; thus, the modification is not located on the lysine residues, but instead on the glutamic acid residue. Interestingly, the peptide ^{61}EETLMEYLENPKK^{73} was again identified; however, the 268 Da addition was found on E^{62}. The b- and y-ion series isolate the modification to E^{61} or E^{62} (Figure 3B). Although manual validation specifies that the modification could occur on either E^{61} or E^{62}, X! Tandem and P-Mod both found the modification on E^{62}. In this case, the low pK_a of this protein region most likely allows for the stability of the 268 Da adduct. The glutamic acid residue is able to adduct NAC-BQ via two possible mechanisms. One possibility is through carboxylate anion formation and stabilization at pH 6. This allows for Michael addition of the γ-carbon to the ring of the BQ (Figure 4A). An additional mechanism of NAC-BQ adduction is through deprotonation of the α-hydrogen, followed by resonance structure formation and stabilization at pH 6 via protonation of the backbone carbonyl. The α-carbon is then able to adduct the BQ ring of NAC-BQ via Michael addition (Figure 4B). Additional experiments have been performed to further confirm the glutamic acid adduction by quinol-thioether metabolites of BQ. Malonic acid, which is structurally similar to glutamic acid, was incubated with NAC-BQ at pH 6, 7, and 8. MS analysis showed that malonic acid was adducted by NAC-BQ via similar chemistry at pH 6 and 7, but not at pH 8 (data not shown).

The reaction of NAC-BQ with cytochrome *c* at pH 7 revealed nine modified peptides (Table 1). The MALDI spectrum for this reaction showed additions of 105 and 268 Da to the protein, and the LC−MS/MS data confirmed this observation. Three of the modified peptides had a mass addition of 268 Da in the reaction at pH 7. The peptides ^{39}KTGQAPGFTYTDANK^{53} and ^{56}GITWKEETLMEYLENPKK^{73} had mass additions of 268 Da on K^{39} and K^{72}, respectively. The y-ion series for the peptide ^{56}GITWKEETLMEYLENPKK^{73} clearly indicates the modification is isolated on residues 71−73, with K^{72} as the likely candidate because of its reactivity in comparison to the proline residue, and because this lysine was missed by tryptic cleavage (Figure 1A of the Supporting Information). Six of the nine modified peptides contained a mass addition of 105 Da. The 105 Da addition was detected on regions of the protein slightly different from that of the 268 Da addition, where the 105 Da adduct occurred mostly on lysine residues adjacent to another lysine residue, either as a direct neighbor or separated by one amino acid (KK or KXK). Because of this motif, and because the 105 Da addition is indicative of the BQ structure, this may indicate that the 105 Da modification can form an adduct linking two neighboring lysine residues or can form an adduct on just a single lysine residue. These observations may indicate that following NAC-BQ binding, stretches of amino acid residues with a high pK_a lead to instability of the adducted NAC-BQ, resulting in postadduction chemistry, which yields the 105 Da adduct. The LC−MS/MS spectrum of the peptide ^{80}MIFAGIKKK^{88} shows the 105 Da addition is located on the C-terminal portion of the peptide (residues 86−88) (Figure 1B of the Supporting Information). The y-ion series of this peptide indicate a mass shift of 105 Da beginning with y_3 and continuing until y_7, and the b-ion series shows a crucial mass shift at b_8. Because this 105 Da addition could link two neighboring lysine residues, K^{86}-K^{87} is the likely position of binding, because K^{88} was recognized as a cleavage site; thus, no modification would likely form at this site. Furthermore, this addition is able to form on a single lysine residue. The peptide ^{39}KTGQAPGFTYTDANKNK^{55} had an addition of 105 Da on $K^{53}-K^{55}$; however, the addition

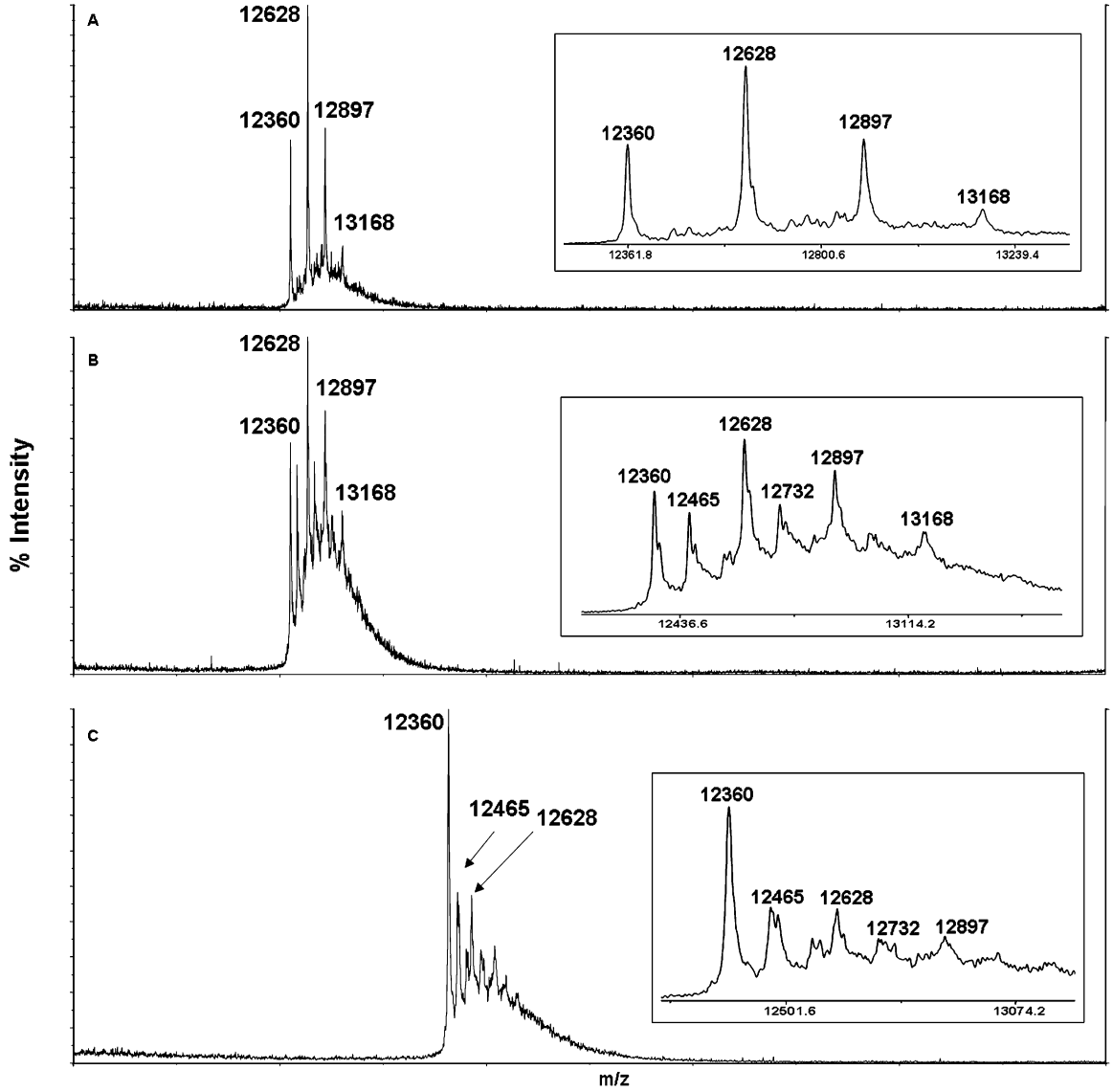

FIGURE 2: MALDI-TOF whole protein spectra for cytochrome *c* reacted with NAC-BQ. (A) Cytochrome *c* was incubated in a buffered pH 6 ammonium acetate/ammonium bicarbonate solution and then reacted with a 1:10 molar ratio of NAC-BQ. The resulting MALDI spectrum shows several additions of 268 Da to cytochrome *c*, corresponding to one addition at *m*/*z* 12 628, two additions at *m*/*z* 12 897, and three additions at *m*/*z* 13 168. (B) Cytochome *c* was incubated in a buffered pH 7 ammonium bicarbonate solution and reacted with a 1:10 molar ratio of NAC-BQ. MALDI analysis reveals additions of both 268 and 105 Da to cytochrome *c*. Peaks at *m*/*z* 12 628, 12 897, and 13 168 correspond to one, two, and three 268 Da mass additions, respectively. The peak at *m*/*z* 12 465 corresponds to one addition of 105 Da, and the peak at *m*/*z* 12 732 corresponds to one addition of 268 Da and one addition of 105 Da. (C) Cytochrome *c* was incubated in a buffered pH 8 ammonium bicarbonate solution and reacted with a 1:10 molar ratio of NAC-BQ. These data revealed additions of 105 and 268 Da; however, the peaks corresponding to the 268 Da additions are low in abundance in comparison to their counterparts at pH 6 and 7. Addionally, the MALDI analysis shows the most predominant peak to be native cytochrome *c*, which may also be a result of NAC-BQ instability at pH 8. The insets in panels A−C are magnified regions of each spectrum.

is most likely isolated on K^{53}, because addition to K^{55} would prevent tryptic cleavage at this site (spectrum not shown). This adduct location illustrates the 105 Da addition to a single residue. Additionally, this adduct position of K^{53} is unique to the 105 Da additions, as no 268 Da additions have been observed at this residue. NAC-BQ thioether bond cleavage following adduction at K^{53} is most likely a result of the adjacent K^{55}, which is attributed to an increase in the surrounding pK_a. However, K^{55} is not spatially oriented to form an adjacent linkage to the HQ ring, and a single 105 Da adduct forms.

Following the reaction of cytochrome *c* and NAC-BQ at pH 8, five tryptic peptides were identified with mass additions of 105 Da (Table 1). The peptide sequences and the site specificity of the 105 Da addition following the reaction at pH 8 match those peptides with 105 Da additions found at pH 7. The b-ion series in the LC−MS/MS spectrum of the peptide ^{23}GGKHKTGPNLHGLFGR^{38} indicate that the 105 Da addition is located on the C-terminal portion of the peptide, and the reactivity of the lysine residues within this portion indicates that the adduct is most likely on K^{25}−K^{27} (Figure 3 of the Supporting Information). No peptides were identified as containing the 268 Da addition following the reaction at pH 8.

Predicted Protein Conformational Changes Associated with NAC-BQ Modification. LC−MS/MS data followed by software analysis and manual validation have indicated that several residues of cytochrome *c* are modified following the

Table 1: Tryptic Peptides Found following the pH-Dependent Reaction of Cytochrome *c* with NAC-BQ[a]

adducts	pH 6	pH 7	pH 8
NAC-BQ 105 adduct	no adducts found	^{6}GK**K**IFVQK^{13} ^{23}GGKH**K**TGPNLHGLFGR^{38} ^{39}KTGQAPGFTYTDANKNK^{55} ^{56}GITWKEETLMEYLENP**K**KYIPGTK^{79} ^{80}MIFAGIK**K**K^{88} ^{87}K**K**TEREDLIAYLK^{99}	^{6}G**K**KIFVQK^{13} ^{23}GGKHKTGPNLHGLFGR^{38} ^{40}TGQAPGFTYTDANKNK^{55} ^{80}MIFAGIK**K**K^{88} ^{87}K**K**TEREDLIAYLK^{99}
NAC-BQ 268 adduct	^{23}GG**K**HKTGPNLHGLFGR^{38} ^{39}**K**TGQAPGFTYTDANK^{53} ^{61}EETLMEYLENP**K**K^{73} ^{61}E**E**TLMEYLENPKK^{73} ^{89}T**E**REDLIAYLKKATNE^{104} ^{92}**E**DLIAYLKK^{100}	^{39}**K**TGQAPGFTYTDANK^{53} ^{56}GITWKEETLMEYLENP**K**K^{73} ^{80}MIFAGIK**K**K^{88}	no adducts found

[a] Bold indicates the residue at which P-Mod or X! Tandem found the modification. Underlined regions consist of residues where manual validation found modification.

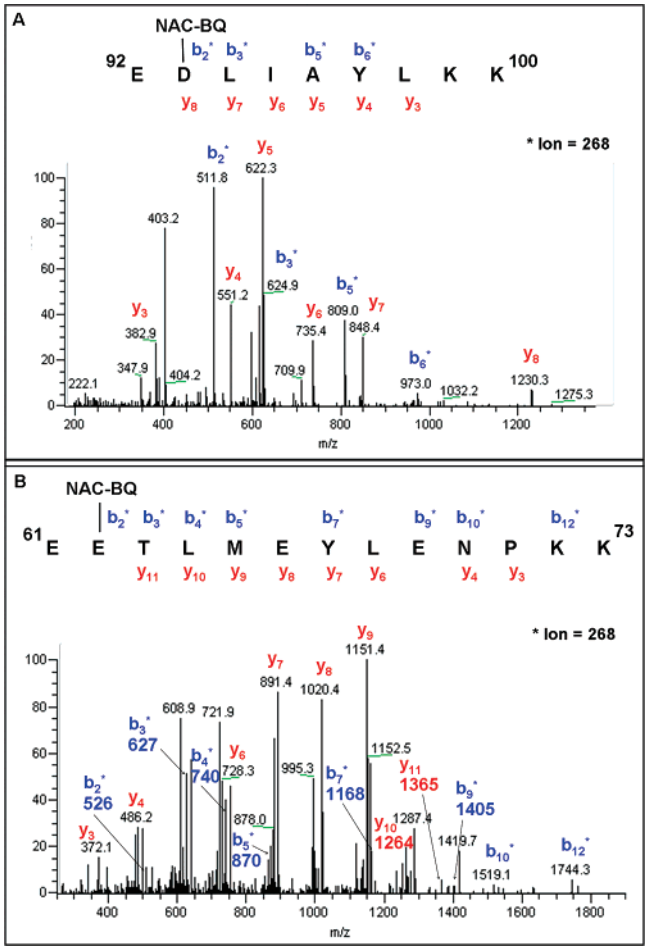

FIGURE 3: MS/MS spectra of cytochrome *c* tryptic peptides modified by NAC-BQ at pH 6. Raw data from LCQ Classic were analyzed using X! Tandem and P-Mod. The resulting adducts were confirmed using manual validation. (A) The cytochrome *c* peptide ^{92}EDLIAYLKK^{100} was adducted by NAC-BQ, where the 268 Da modification was located on E^{92}. (B) The cytochrome *c* peptide ^{61}EETLMEYLENPKK^{73} had the 268 Da modification on E^{62}.

reaction of NAC-BQ with cytochrome *c*. Like BQ, NAC-BQ may also inhibit apoptosome formation by inducing conformational changes in critical residues involved in cytochrome *c*−Apaf-1 binding. The 268 Da NAC-BQ modification was added to E^{62} (Figure 5), on the basis of the results of the reaction of NAC-BQ and cytochrome *c* at pH 6. The reaction at pH 7 also indicated formation of a 268 Da addition to K^{72} and a 105 Da addition to K^{86}-K^{87}, so these models were also constructed (panels A and B of Figure 2 of the Supporting Information, respectively). The results of the reaction at pH 8 indicated formation of a 105 Da addition to K^{25}−K^{27}, and a stable model of this modification was also constructed (Figure 4 of the Supporting Information). Subsequent energy minimizations and dynamics were performed, and the effect of the NAC-BQ modification could be assessed through conformational rearrangement of certain residues within cytochrome *c*. In the case of K^{25}−K^{27} and K^{86}-K^{87}, a cyclic BQ species is added, which links both residues at opposite sides of the BQ ring structure. Again, the critical residues involved in binding Apaf-1 are highlighted for viewing of any additional conformational changes in these residues following NAC-BQ addition.

Circular Dichroism Spectroscopy following Modification of Cytochrome c with BQ and NAC-BQ. Following the reaction of cytochrome *c* with BQ and NAC-BQ (Materials and Methods), far-UV spectroscopy was used to establish whether the secondary structures of BQ-adducted cytochrome *c* and NAC-BQ-adducted cytochrome *c* were significantly different from that of native cytochrome *c* (Figure 6). Molecular modeling of the modified and native cytochrome *c* predicted structural changes associated with the modifications, and further structural data were necessary to support the results of the modeling studies. Functional studies measuring caspase activity following modification of cytochrome *c* with BQ have also indicated that the biological function of this protein is altered upon BQ modification (see below). Consequently, we determined whether the secondary structure of the protein remained intact following BQ and NAC-BQ modifications. CD spectra were measured to determine whether the BQ and/or NAC-BQ modifications induced sufficient conformational changes to result in significant misfolding of the protein secondary structure, which might be responsible for the inhibition of protein function. The CD spectra of BQ- and NAC-BQ-adducted cytochrome *c* appear similar to the native spectrum with no significant visible band shifts between the spectra. To further investigate the structural changes associated with this chemical adduction on cytochrome *c*, intrinsic fluorescence measurements were conducted using the samples prepared for CD analysis; however, the proximity of the tryptophan

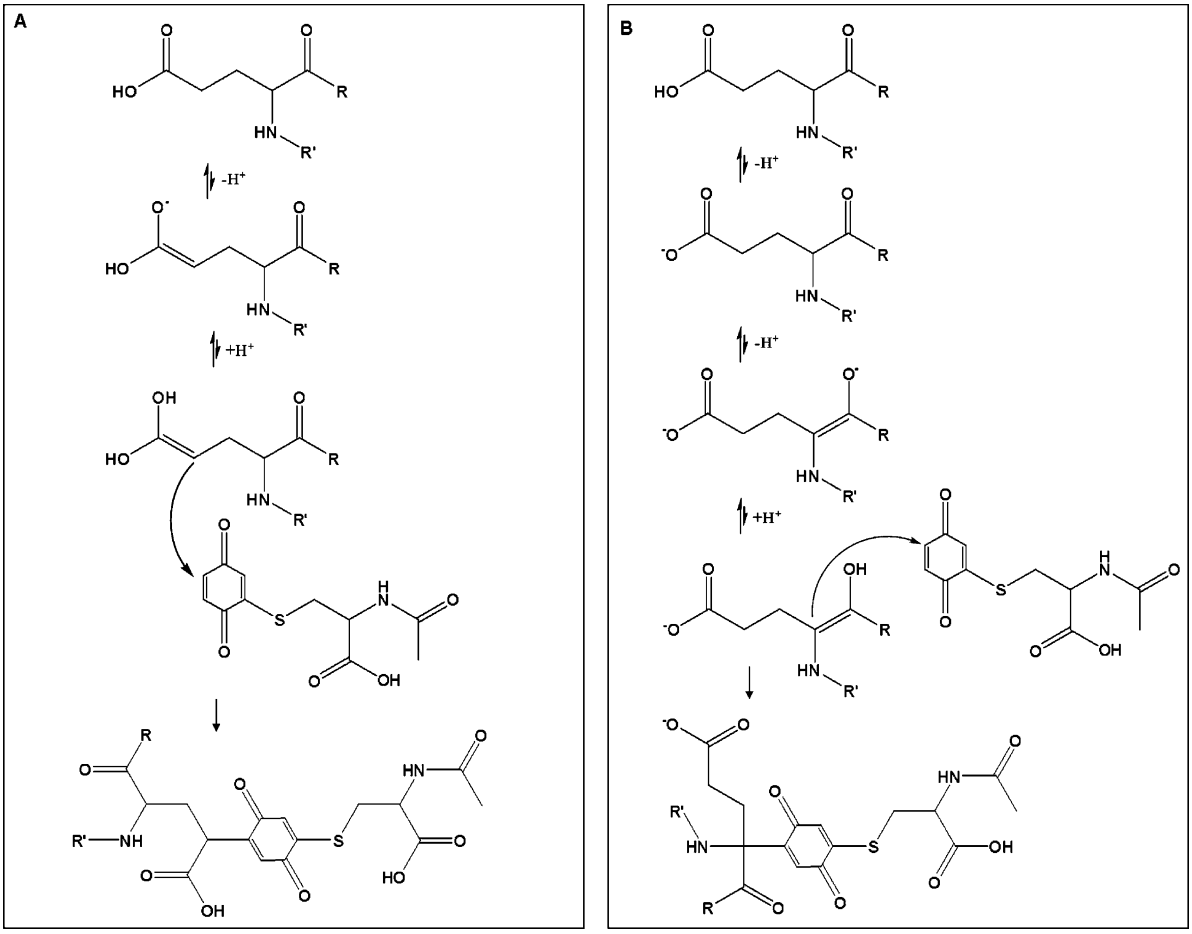

FIGURE 4: NAC-BQ 268 Da adduction on glutamic acid residues at pH 6. (A) The glutamic acid forms an enolate anion where the electron density is shared between both oxygen atoms and is then protonated at pH 6 to a more stable species. The γ-carbon is then capable of adducting the BQ ring via Michael addition. (B) Deprotonation of the α-hydrogen of the glutamic acid residue allows for resonance structure formation, which is stabilized at pH 6 via protonation of the backbone carbonyl. The α-carbon is then able to adduct the BQ ring of NAC-BQ through Michael addition.

residue to the heme in cytochrome *c* likely resulted in quenching of the tryptophan fluorescence (data not shown). Therefore, the CD results indicate that the BQ- and NAC-BQ-induced PTMs likely create subtle structural rearrangements of critical residues involved in the normal functioning of the protein, and with spatial rearrangement of these critical residues, the biological activity of cytochrome *c* is altered. The samples used for CD analysis were analyzed via MALDI-TOF analysis to ensure modifications of cytochrome *c* by BQ and NAC-BQ.

Adduction of 1,4-Benzoquinone to Cytochrome c Inhibits Formation of the Apaf-1 Apoptosome and Activation of Caspase-9 and -3. Next, we examined the ability of native and BQ-adducted cytochrome *c* to initiate formation of the Apaf-1 apoptosome and sequential activation of caspase-9 and -3 in naïve human monocytic THP.1 tumor cell lysates and in an entirely reconstituted apoptosome model. The addition of native cytochrome *c* to THP.1 lysates led to a concentration-dependent increase in caspase-3 DEVDase activity, implying that cytochrome *c* had induced formation of the Apaf-1·caspase-9 apoptosome, which in turn activated procaspase-3 (DEVDase activity). By contrast, no significant increase in DEVDase activity was observed in lysates incubated with BQ-adducted cytochrome *c* (Figure 7A). To confirm that BQ-adducted cytochrome *c* could not activate the apoptosome, we reconstituted the complex with recombinant Apaf-1, procaspase-9, procaspase-3, and either native or BQ-adducted cytochrome *c*. As expected, native cytochrome *c* induced oligomerization of Apaf-1 and consequently activated caspase-9 and -3, resulting in caspase-3 DEVDase activity. However, adducted cytochrome *c* failed to induce Apaf-1 oligomerization and consequently failed to activate caspases (Figure 7B,C).

DISCUSSION

Cytochrome *c* has been utilized as a model protein to characterize chemical-induced post-translational modifications (PTMs) on the protein resulting from reaction with BQ and NAC-BQ. Additionally, because intact cytochrome *c* is critical for the normal function of the stress-induced apoptosis pathway, site-specific modification of residues within this protein could disrupt essential protein−protein interactions required for the initiation of cell death. Moreover, the MS data were analyzed to determine whether reactive electrophiles preferentially target specific amino acids on the basis of the orientation of the amino acids and on the basis of the chemical and physical properties of the solvent-exposed residues within the protein. Identification of potential preferential binding characteristics may facilitate selective adduction on certain amino acid residues, based upon specific electrophile binding motifs (EBM) within proteins. Potential quinone EBMs have previously been identified as containing

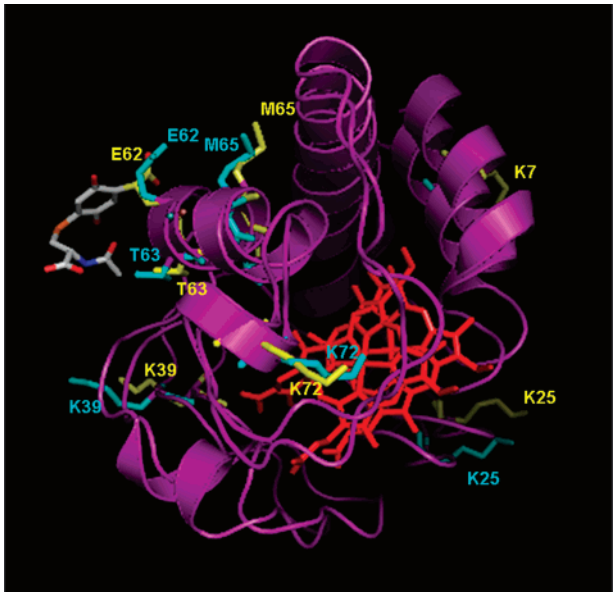

FIGURE 5: Molecular model of cytochrome *c* following covalent adduction by NAC-BQ at E^{62}. MS/MS data provided results showing the NAC-BQ 268 Da adduct was located on E^{62} following the reaction at pH 6. The model was created using Insight II. Following molecular dynamics and energy minimizations, the lowest-potential energy structure was placed in PyMOL. The modified protein (yellow residues) is overlaid with the native protein (blue residues) to observe spatial rearrangement of critical residues involved in cytochrome *c* function. Residues highlighted in the modified and native proteins are those crucial for binding of cytochrome *c* to Apaf-1.

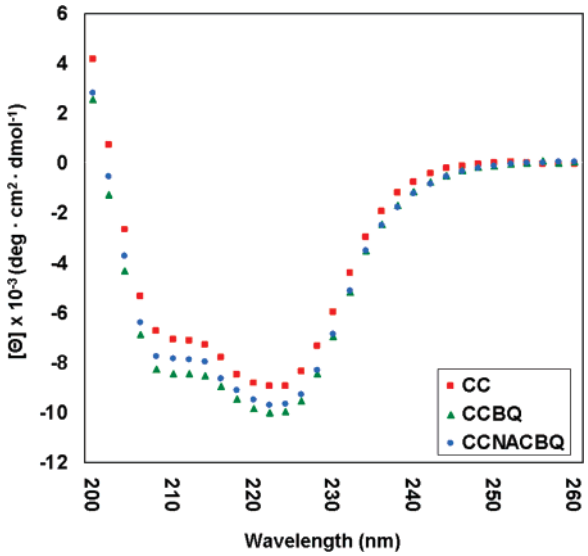

FIGURE 6: Far-UV circular dichroism of BQ- and NAC-BQ-adducted cytochrome *c*. The CD spectra of the BQ-adducted cytochrome *c* (green triangles) and the NAC-BQ-adducted cytochrome *c* (blue circles) are shown with the spectrum of the native cytochrome *c* structure (red squares).

runs of lysine residues in a specific orientation, generally including two lysine residues flanking a nucleophilic amino acid (KXK) or two lysine residues preceded or followed by a nucleophilic amino acid (XKK or KKX). Proteins containing these EBMs may be predisposed to BQ- and NAC-BQ-mediated modification, leading to alterations in structural and possibly functional characteristics. Site-directed mutagenesis studies have revealed that cytochrome *c* forms complexes with Apaf-1 through specific interaction with residues K^7, K^{25}, K^{39}, ^{62}ETLM^{65}, and K^{72} (*27*). Selective binding of BQ and/or NAC-BQ to any of these cytochrome *c* residues may disrupt the cytochrome *c*−Apaf-1 interaction. Modification of one of these residues involved in cytochrome *c*−Apaf-1 interaction decreases the level of caspase-3 activation (*27*). However, modification of multiple residues involved in this interaction or a change in the spatial orientation of these critical residues as a result of binding elsewhere on the protein has an additive effect on the decrease in the level of caspase-3 activation, and thus the ability of cytochrome *c* to initiate the apoptosis pathway (*16*, *17*, *28*). Interestingly, several of the reactive electrophile-induced PTMs we have identified are located on K^7, K^{25}, K^{39}, E^{62}, and K^{72}. Because these residues are crucial contributors to protein−protein interactions, their modification by BQ or any of its quinol-thioether metabolites may cause a significant decrease in the level of cytochrome *c* binding and caspase-3 activity. Additionally, modification at these sites by BQ, or any of its quinol-thioether metabolites, may contribute to inhibition of Apaf-1 oligomerization necessary for apoptosome formation (Figure 7).

The pH dependence of the reaction of cytochrome *c* with quinol-thioether metabolites of BQ was investigated to determine whether pH influences the nature and/or selectivity of protein modification. MALDI-MS and LC−MS/MS analysis revealed that these NAC-BQ adducts do form in a pH-dependent manner on solvent-exposed cytochrome *c* residues. This analysis has revealed that following reaction of NAC-BQ with cytochrome *c*, 268 Da adducts are found at pH 6 and 7, but 105 Da adducts are found at pH 7 and 8 (Figure 2). The observed pH dependence is likely due to the instability of the protein-adducted NAC-BQ at increasing pH values, where the final 105 Da addition occurs as a result of postadduction chemistry following binding of NAC-BQ at these residues. Thus, elimination of the *N*-acetylcysteine moiety from the BQ ring gives rise to the 105 Da adduct observed at increasing pH values. The postadduction chemistry that occurs to give the 105 Da adduct is observed mostly on amino acids that are surrounded by regions with a high pK_a, whereas the 268 Da adducts are observed in protein regions with a lower pK_a. These regions with a low pK_a appear to stabilize the 268 Da adduct, preventing elimination of the *N*-acetylcysteine moiety. In addition to the lysine residues that have been shown to be targets of these electrophilic compounds, we have identified glutamic acid as a novel residue modified by NAC-BQ at pH 6 (Figure 3). Only glutamic acid residues that are surrounded by regions with a low pK_a are sites of the 268 Da adduction, further signifying the importance of pK_a in quinol thioether adduct formation and the associated postadduction chemistry. Additionally, this novel adduction site further characterizes protein targets of quinone compounds and helps elucidate their mechanisms of binding.

Protein modeling of BQ and NAC-BQ modification on cytochrome *c* was conducted to predict structural changes in the protein conformation following covalent modification by these compounds. Modeling BQ and NAC-BQ adduction to cytochrome *c* on critical lysine (Figure 1) and glutamic acid (Figure 5) residues revealed a change in the orientation of these residues for accommodation of the quinone adducts (postulated structures of these chemical adducts are found in Figure 5 of the Supporting Information). This structural

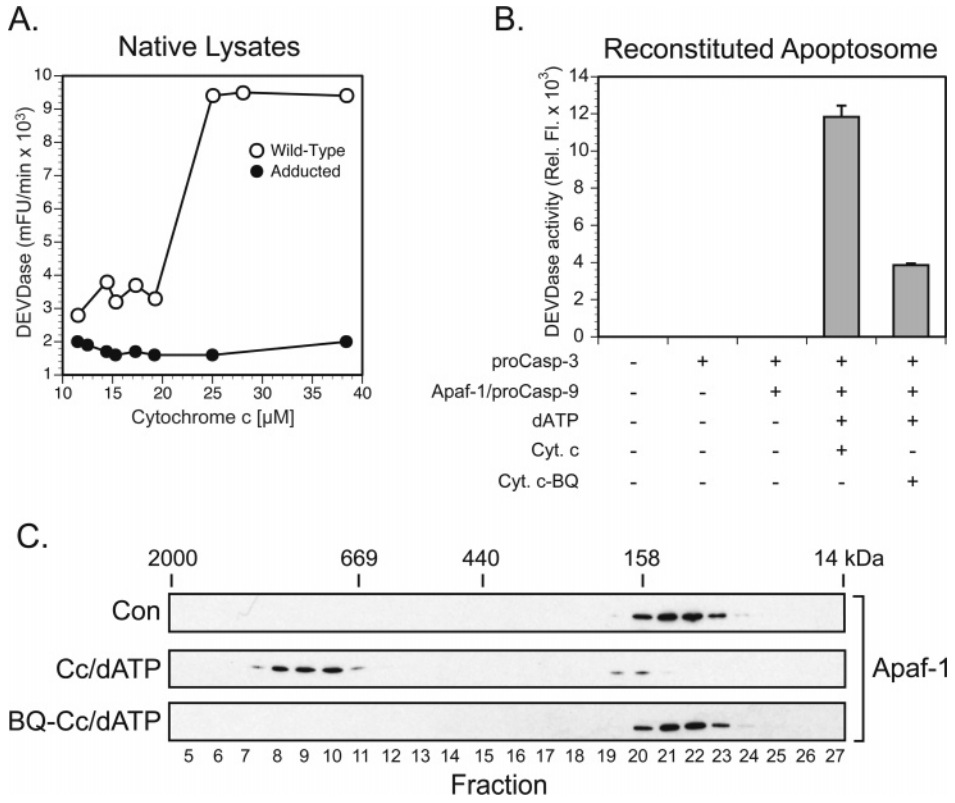

FIGURE 7: Adduction of cytochrome *c* with BQ inhibits formation of the Apaf-1 apoptosome and prevents caspase activation. (A) THP-1 lysates were activated with dATP in the presence of increasing concentrations of cytochrome *c* or BQ-adducted cytochrome *c*. Apoptosome-mediated activation of procaspase-3 was assessed using the caspase-3 substrate, DEVD-AMC. (B and C) Native and BQ-adducted cytochrome *c* were examined for their abilities to induce oligomerization of recombinant Apaf-1 into an apoptosome complex, capable of activating procaspase-9 and -3.

adjustment induced subsequent changes in the spatial orientation of additional residues within cytochrome *c*, particularly those residues which facilitate the cytochrome *c*−Apaf-1 protein−protein interactions. This observed structural rearrangement following adduction by these quinone compounds suggests one possible mechanism for the inhibition of the interaction of cytochrome *c* with Apaf-1, resulting in inhibition of cytochrome *c*-initiated caspase activation. Alternatively, it is possible that BQ and its quinol-thioether metabolites induce global changes in cytochrome *c* conformation sufficient to produce a loss of protein function. In this case, the more subtle local conformational changes affecting only the spatial orientation of specific residues would likely be overwhelmed by the consequences of gross changes in protein structure. However, circular dichroism (CD) analysis of the BQ- and NAC-BQ-modified cytochrome *c* revealed that the secondary structure of the protein remains essentially intact following modification (Figure 6). These data therefore suggest that reactive electrophile-induced PTMs cause a loss of protein function in the absence of gross alterations in protein structure. Thus, the spatial rearrangement of the affected residues following this quinone adduction on cytochrome *c* is sufficient to inhibit cytochrome *c* protein−protein interactions, and thus loss of protein function.

Adduction to any site on cytochrome *c* that is involved in protein−protein interactions may be sufficient to produce a loss of protein function independent of any structural changes. Recent literature has demonstrated that negatively charged nucleotides bind to cytochrome *c* likely through electrostatic interactions and that these nucleotides interfere with cytochrome *c*-initiated caspase activation (*29*, *30*). The authors suggest that the nucleotides interact at the same sites on cytochrome *c* necessary for Apaf-1 binding and are therefore able to inhibit cytochrome *c*-initiated caspase activation by preventing protein−protein interactions without the associated structural rearrangements. Because we have shown that BQ and its quinol-thioether metabolites bind to many of the same sites on cytochrome *c* known to be crucial for Apaf-1 interaction, the simple masking of these protein−protein interaction sites may be sufficient to cause a loss of function independent of any local conformational changes.

In summary, BQ and its quinol-thioether metabolites (NAC-BQ) are capable of creating PTMs in cytochrome *c* that alter protein structure. In addition, the nature of the chemical adduct is dependent on the physicochemical characteristics at the site of adduction. Thus, postadduction chemistry can result in rearrangements that may render invalid assumptions about the proposed structure of chemical-induced PTMs. However, despite such difficulties, identification of EBMs recognized by specific classes of reactive electrophilic metabolites should assist in directing the search for chemical-induced PTMs, and the consequences thereof. In this respect, BQ- and NAC-BQ-induced PTMs in cytochrome *c* produce changes in the structure of cytochrome *c* sufficient to inhibit its ability to promote the processing of caspase-3 by the apoptosome. The contribution of chemical-induced PTMs to the toxicity associated with chemical exposure remains to be determined but will likely involve multiple protein targets. Assessing which, if any, of these PTMs alter structure and function sufficient to influence cell viability remains a challenge.

ACKNOWLEDGMENT

We are grateful to Dr. Bogdan Olenyuk, Department of Chemistry, for chemical adduct guidance and to Dr. Laurence Hurley, Division of Medicinal Chemistry, for use of circular dichroism spectroscopy instrumentation. We also thank Dr. Howard Fearnhead (National University of Ireland, Galway, Ireland) for kindly providing the Apaf-1XL-expressing baculovirus and Dr. G. M. Cohen for providing the Apaf-1 antibody (MRC Toxicology Unit, Leicester, U.K.). Special thanks to the Southwest Environmental Health Sciences Proteomic Core Facility for assistance in acquisition of mass spectra.

SUPPORTING INFORMATION AVAILABLE

Additional information as described in the text, including mass spectral data for several additional cytochrome *c* tryptic peptides showing modifications and the corresponding structural predictions of these site-specific modifications to cytochrome *c*. This material is available free of charge via the Internet at http://pubs.acs.org.

REFERENCES

1. Cohen, S. D., Pumford, N. R., Khairallah, E. A., Boekelheide, K., Pohl, L. R., Amouzadeh, H. R., and Hinson, J. A. (1997) Selective protein covalent binding and target organ toxicity, *Toxicol. Appl. Pharmacol. 143*, 1−12.
2. Zhou, S., Chan, E., Duan, W., Huang, M., and Chen, Y. Z. (2005) Drug bioactivation, covalent binding to target proteins and toxicity relevance, *Drug Metab. Rev. 37*, 41−213.
3. Person, M. D., Mason, D. E., Liebler, D. C., Monks, T. J., and Lau, S. S. (2005) Alkylation of cytochrome c by (glutathion-S-yl)-1,4-benzoquinone and iodoacetamide demonstrates compound-dependent site specificity, *Chem. Res. Toxicol. 18*, 41−50.
4. Person, M. D., Monks, T. J., and Lau, S. S. (2003) An integrated approach to identifying chemically induced posttranslational modifications using comparative MALDI-MS and targeted HPLC-ESI-MS/MS, *Chem. Res. Toxicol. 16*, 598−608.
5. Guengerich, F. P., and Liebler, D. C. (1985) Enzymatic activation of chemicals to toxic metabolites, *Crit. Rev. Toxicol. 14*, 259−307.
6. Ross, D. (2000) The role of metabolism and specific metabolites in benzene-induced toxicity: Evidence and issues, *J. Toxicol. Environ. Health, Part A 61*, 357−372.
7. Pagano, G. (2002) Redox-modulated xenobiotic action and ROS formation: A mirror or a window? *Hum. Exp. Toxicol. 21*, 77−81.
8. Bolton, J. L., Trush, M. A., Penning, T. M., Dryhurst, G., and Monks, T. J. (2000) Role of quinones in toxicology, *Chem. Res. Toxicol. 13*, 135−160.
9. Verrax, J., Delvaux, M., Beghein, N., Taper, H., Gallez, B., and Buc Calderon, P. (2005) Enhancement of quinone redox cycling by ascorbate induces a caspase-3 independent cell death in human leukaemia cells. An in vitro comparative study, *Free Radical Res. 39*, 649−657.
10. Ruiz-Ramos, R., Cebrian, M. E., and Garrido, E. (2005) Benzoquinone activates the ERK/MAPK signaling pathway via ROS production in HL-60 cells, *Toxicology 209*, 279−287.
11. Lindsey, R. H., Jr., Bender, R. P., and Osheroff, N. (2005) Effects of benzene metabolites on DNA cleavage mediated by human topoisomerase IIα: 1,4-Hydroquinone is a topoisomerase II poison, *Chem. Res. Toxicol. 18*, 761−770.
12. Lau, S. S., Hill, B. A., Highet, R. J., and Monks, T. J. (1988) Sequential oxidation and glutathione addition to 1,4-benzoquinone: Correlation of toxicity with increased glutathione substitution, *Mol. Pharmacol. 34*, 829−836.
13. Peters, M. M., Jones, T. W., Monks, T. J., and Lau, S. S. (1997) Cytotoxicity and cell-proliferation induced by the nephrocarcinogen hydroquinone and its nephrotoxic metabolite 2,3,5-(tris-glutathion-S-yl)hydroquinone, *Carcinogenesis 18*, 2393−2401.
14. Kleiner, H. E., Jones, T. W., Monks, T. J., and Lau, S. S. (1998) Immunochemical analysis of quinol-thioether-derived covalent protein adducts in rodent species sensitive and resistant to quinol-thioether-mediated nephrotoxicity, *Chem. Res. Toxicol. 11*, 1291−1300.
15. Yoon, H. S., Monks, T. J., Walker, C. L., and Lau, S. S. (2001) Transformation of kidney epithelial cells by a quinol thioether via inactivation of the tuberous sclerosis-2 tumor suppressor gene, *Mol. Carcinog. 31*, 37−45.
16. Bratton, S. B., Walker, G., Srinivasula, S. M., Sun, X. M., Butterworth, M., Alnemri, E. S., and Cohen, G. M. (2001) Recruitment, activation and retention of caspases-9 and -3 by Apaf-1 apoptosome and associated XIAP complexes, *EMBO J. 20*, 998−1009.
17. Bratton, S. B., Walker, G., Roberts, D. L., Cain, K., and Cohen, G. M. (2001) Caspase-3 cleaves Apaf-1 into an approximately 30 kDa fragment that associates with an inappropriately oligomerized and biologically inactive approximately 1.4 MDa apoptosome complex, *Cell Death Differ. 8*, 425−433.
18. Craig, R., and Beavis, R. C. (2003) A method for reducing the time required to match protein sequences with tandem mass spectra, *Rapid Commun. Mass Spectrom. 17*, 2310−2316.
19. Craig, R., Cortens, J. P., and Beavis, R. C. (2004) Open source system for analyzing, validating, and storing protein identification data, *J. Proteome Res. 3*, 1234−1242.
20. Hansen, B. T., Davey, S. W., Ham, A. J., and Liebler, D. C. (2005) P-Mod: An algorithm and software to map modifications to peptide sequences using tandem MS data, *J. Proteome Res. 4*, 358−368.
21. Standing, K. G. (2003) Peptide and protein de novo sequencing by mass spectrometry, *Curr. Opin. Struct. Biol. 13*, 595−601.
22. Bushnell, G. W., Louie, G. V., and Brayer, G. D. (1990) High-resolution three-dimensional structure of horse heart cytochrome c, *J. Mol. Biol. 214*, 585−595.
23. *Insight II* (2000) Accelrys Inc., San Diego.
24. Discover_3 ESFF (extensible systematic force field). Molecular mechanics force fields, *Insight II, 2000.3L* (2000) Accelrys, Inc., San Diego.
25. Jorgensen, W. L., Chandrasekhar, J., Madura, J. D., Impey, R. W., and Klein, M. L. (1983) Comparison of simple potential functions for simulating liquid water, *J. Chem. Phys. 79*, 926−935.
26. Cain, K., Bratton, S. B., Langlais, C., Walker, G., Brown, D. G., Sun, X. M., and Cohen, G. M. (2000) Apaf-1 oligomerizes into biologically active approximately 700-kDa and inactive approximately 1.4-MDa apoptosome complexes, *J. Biol. Chem. 275*, 6067−6070.
27. Yu, T., Wang, X., Purring-Koch, C., Wei, Y., and McLendon, G. L. (2001) A mutational epitope for cytochrome C binding to the apoptosis protease activation factor-1, *J. Biol. Chem. 276*, 13034−13038.
28. Shi, Y. (2002) Apoptosome: The cellular engine for the activation of caspase-9, *Structure 10*, 285−288.
29. Chandra, D., Bratton, S. B., Person, M. D., Tian, Y., Martin, A. G., Ayres, M., Fearnhead, H. O., Gandhi, V., and Tang, D. G. (2006) Intracellular nucleotides act as critical prosurvival factors by binding to cytochrome c and inhibiting apoptosome, *Cell 125*, 1333−1346.
30. Samali, A., O'Mahoney, M., Reeve, J., Logue, S., Szegezdi, E., McMahon, J., and Fearnhead, H. O. (2007) Identification of an inhibitor of caspase activation from heart extracts: ATP blocks apoptosome formation, *Apoptosis 12*, 465−474.

BI700613W